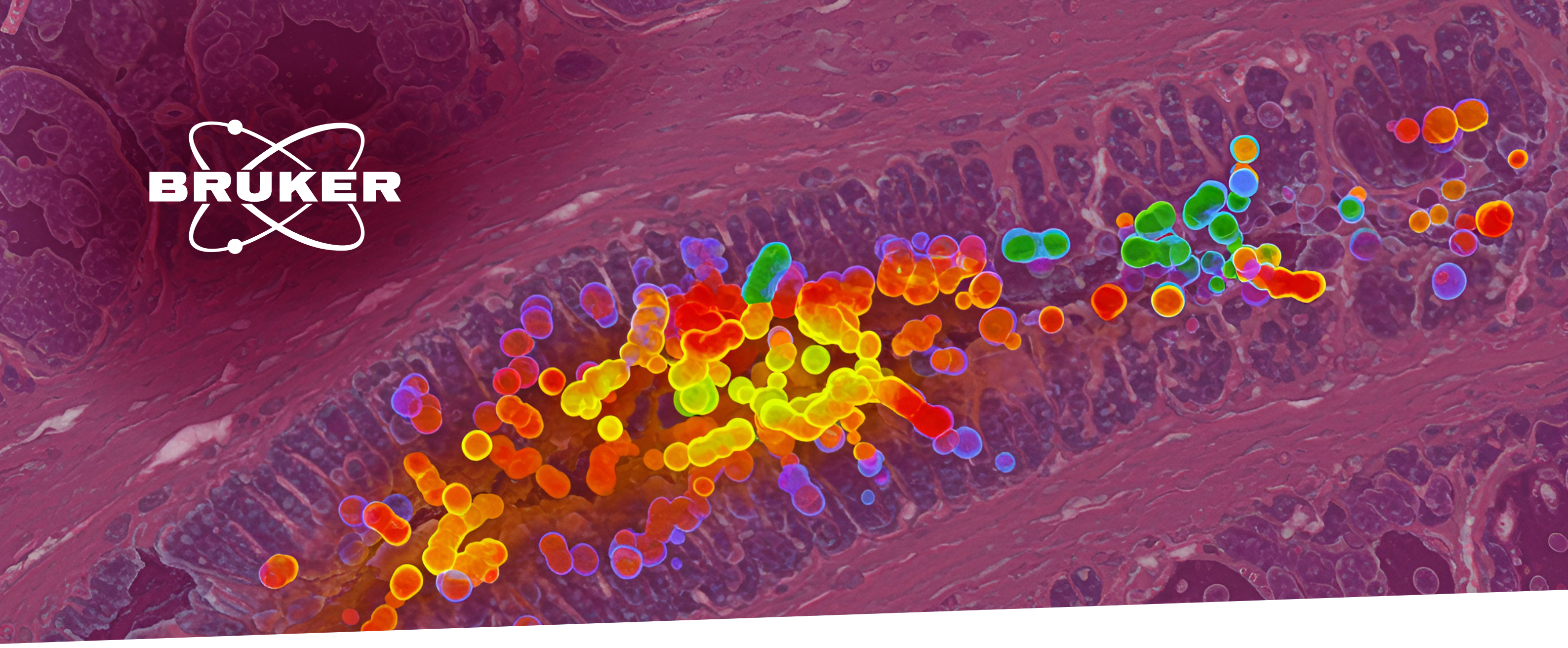

From Spatial Biology Glycomic Imaging to High Resolution Glycoproteomics: Integrating GlycoPath MALDI-MSI and glyco-PASEF Glycopeptide LC-MS/MS

Spatially guided glycopeptide profiling enabled by integrated imaging and PASEF®-based LC-MS/MS for tissue-level glycosylation mapping

Abstract

Glycosylation plays a central role in maintaining protein structure and function, particularly in cell-cell communication and immune signaling. In this study, we integrate high-resolution mass spectrometry imaging (MSI) of released glycans with intact glycopeptide analysis to uncover spatial and molecular differences in N-glycosylation between tumor and normal prostate tissue, and to connect and resolve findings from glycomics spatial biology imaging with commensurate observations on the level of individual glycoprotein analysis. MALDI-MSI revealed prominent changes in glycan spatial distribution, including enrichment of high-mannose and bisected glycans in tumor tissue, while complex-type fucosylated and sialylated glycans predominated in normal regions. LC-MS/MS analysis of glycopeptides validated these trends and highlighted specific glyco-proteins involved. This dual-modality approach provides mechanistic insights into glycosylation remodeling during malignant transformation and strongly indicates the potential relevance of glycosylation-specific biomarkers.

Keywords:
Glycomics, Glycopeptides, Glycoproteomics, N-glycosylation, Glycomics Spatial Biology, Glycobiology, Prostate Cancer, HILIC

Introduction

N-glycosylation is a conserved post-translational modification that influences protein folding, trafficking, and cell-surface interactions. The composition and structure of N-glycans can vary depending on cellular context, including cancer, where it has long been recognized, but not well characterized so far, that profound changes in protein glycosylation commonly occur. For instance, high-mannose structures can accumulate (likely due to endoplasmic reticulum stress), and incomplete glycan maturation is observed, while complex-type glycans with sialylation and fucosylation reflect full maturation in the Golgi.

Hongxia Bai, Grace Grimsley, Klaus Lindpaintner, Bruker Scientific LLC, Billerica, MA, USA.

Spatial biology glycomic studies using MALDI-MSI allow visualization of glycan species directly within tissue architecture, maintaining their anatomical context and preserving information content on regional heterogeneity. This is particularly powerful when paired with histology, as MSI signals can be aligned to specific morphological features such as glands, ducts, or tumor borders. In contrast, glycoproteomic analysis by LC-MS/MS typically involves tissue homogenization and peptide extraction, sacrificing spatial context but enabling in-depth molecular characterization of glycosylation micro- and macro-heterogeneity, i.e. information on glycan structures and their respective localization to individual glycosylation sites across a broader dynamic range.

Here, we present an integrated workflow combining MALDI-MSI using the timsTOF fleX and glyco-PASEF-based LC-MS/MS using the timsTOF Ultra 2. Tissue sections from matched tumor and normal prostate samples were analyzed to map glycan distribution and identify specific glycopeptide species. This integrated approach newly bridges the spectrum from anatomy and histology to molecular pathology all the way to sub-molecular biochemistry in glycobiology, enabling highly interdisciplinary, detailed and comprehensive new biomedical insights into the spatial and molecular aspects of glycosylation in cancer.

Materials and Methods

Sample Preparation and MALDI-MSI Acquisition

Formalin-fixed paraffin-embedded (FFPE) tissue sections from prostate cancer (PCa) and normal tissue were prepared for MALDI mass spectrometry imaging (MSI) following a standardized workflow. Slides were first dewaxed by incubation at 60°C for 1 hour, then sequentially immersed in xylene (2 × 3 minutes), 100% ethanol (2 × 1 minute), 95% ethanol (1 × 1 minute), 70% ethanol (1 × 1 minute), and HPLC-grade water (2 × 3 minutes) to remove paraffin and rehydrate the tissue.

Subsequently, antigen retrieval was carried out by steaming the slides for 30 minutes in citraconic acid buffer at pH 3 using a vegetable steamer. After cooling, tissues were uniformly coated with PNGase F at a concentration of 0.1 μg/mL to release N-linked glycans. Enzymatic digestion proceeded for 2 hours at 37°C in a humidity chamber. A matrix solution of α-cyano-4-hydroxycinnamic acid (CHCA) at 7 mg/mL was then applied uniformly to the slides.

MSI was conducted on a timsTOF fleX instrument using a 40 μm raster step size, a 20 μm × 20 µm laser spot, and 300 laser shots per pixel. Mass spectra were acquired over the m/z range of 700 to 4000. Raw data were processed in SCiLS Lab software and normalized to total ion current to enable comparative spatial analysis across samples.

Glycopeptide Extraction

Adjacent tissue sections were dewaxed and deparaffinized using the same protocol. After drying in a desiccator, the tissue was scraped from the slides using a sterile razor blade and transferred into centrifuge tubes. Samples were homogenized using a BeatBox homogenizer (PreOmics) at high speed for 10 minutes, then incubated at 95°C for 1 hour in lysis buffer (PreOmics iST Kit 8x). The homogenization step was repeated once to ensure thorough lysis. The resulting homogenates were processed according to the PreOmics iST Kit protocol, including reduction, alkylation, enzymatic digestion, and peptide cleanup.

Glycopeptides were enriched using Agilent AssayMAP Bravo with HILIC cartridges, following the procedure previously described (AppNote 1918673-LCMS-239). Stepwise elution was performed using decreasing ACN concentrations (75%, 70%, 65%) and 0.5% formic acid. Eluates were pooled, dried, and resuspended for analysis.

LC-MS/MS Analysis

Peptides were separated on an IonOpticks Aurora C18 column (25 cm × 75 μm) using a nanoElute® 2 system at 0.25 μL/min. A 67.27-minute gradient from 2% to 95% acetonitrile was applied. Data were acquired using a stepped glyco-PASEF method with 6 PASEF scans per 1.38 s cycle. TIMS range was set as $1/K_0$ = 0.80–1.60 Vs/cm^2. CID energies: 35–54 eV and 40–100 eV. Instrument parameters were tuned for glycopeptide fragmentation. Detailed instrument parameters can be found in a published App Note (AppNote 1918673-LCMS-239).

Results and Discussions

Hematoxylin and eosin (H&E) staining (Figure 1A) confirmed distinct histological differences between tumor and normal prostate tissues. Normal prostate tissue exhibited well-organized glandular architecture, while prostate cancer (PCa) sections showed disorganized, hypercellular morphology consistent with malignant transformation. Average spectra from MALDI-MS glycomic profiling (Figure 1B) revealed striking differences in glycan abundance and composition between normal and tumor tissues. Notably, high-mannose glycans such as Man5 (N2H5) and core-fucosylated biantennary glycans (N4H5F1) were abundant in normal samples, while PCa samples showed a high presence of sialylated and branched glycans, such as N4H5S2 and N2H6.

The spatial heatmaps in Figure 2 reveal striking differences in glycan localization and abundance between normal and tumor prostate tissues. In normal samples, biantennary glycans are strongly localized to stromal compartments, likely reflecting glycosylated extracellular matrix (ECM) proteins such as fibronectin or laminin, or secretory glycoproteins produced by fibroblasts. Their presence in these connective areas may contribute to maintaining tissue structure, cell adhesion, or growth factor modulation. Interestingly, this stromal enrichment is attenuated in tumor samples, where signals are generally more diffuse and less structured. This spatial flattening may be indicative of a disrupted microenvironment, altered fibroblast activity, or reduced ECM glycoprotein production in the tumor-associated stroma.

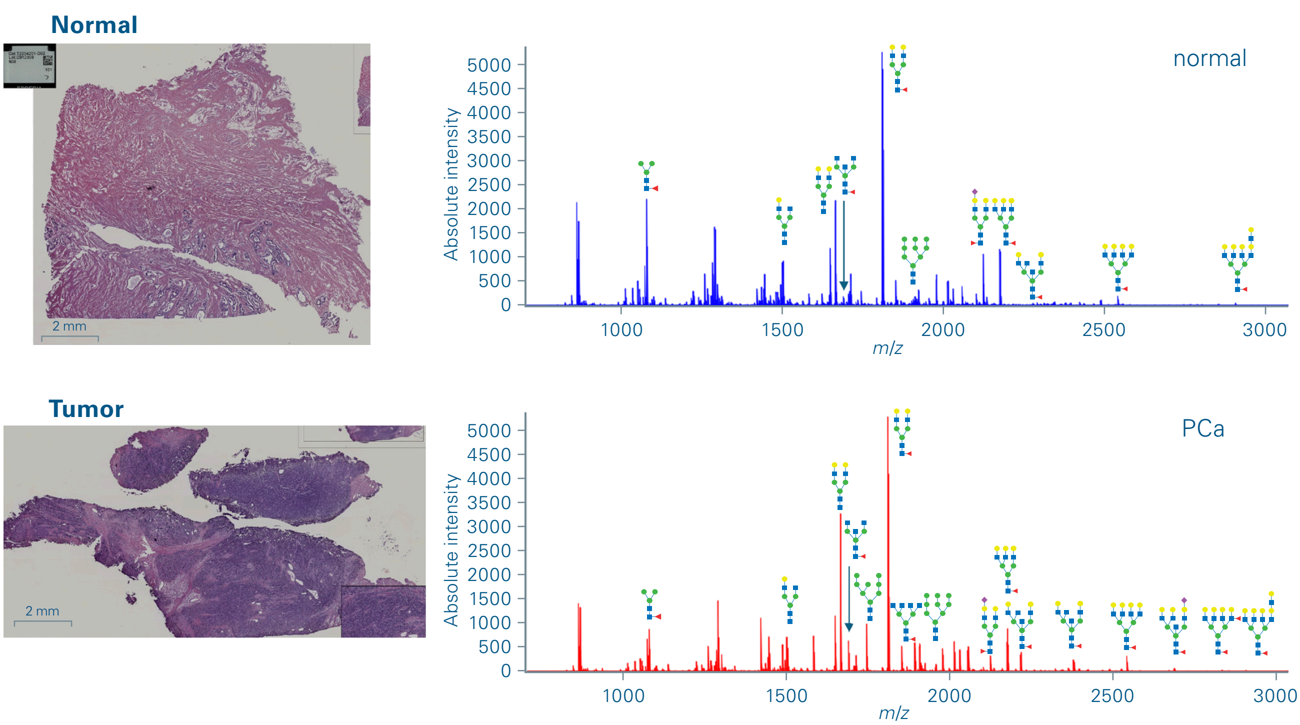

Figure 1.

Histology and MALDI-MS glycan profiling of normal (upper image and spectrum) and prostate cancer (PCa, lower image and spectrum) tissue.

Figure 2. **Spatial distribution of representative N-glycan classes across normal and tumor prostate tissues.**
In each vignette, the upper section represents normal tissue, the lower PCa tissue; purple color indicates lower abundance, and yellow color indicates higher abundance of the correspondingly shown glycan.

Hybrid glycans, particularly those with both high-mannose and complex features, also exhibit stronger signals in normal tissue. Their reduced representation in tumors may reflect shifts in Golgi processing efficiency or branching enzyme activity, consistent with the deregulated glycosylation pathways frequently observed in cancer. The loss of such species might impact protein folding, stability, or trafficking, further exacerbating tumor progression.

In contrast, tumor samples show modest increases in certain complex or highly branched glycans, though with less defined spatial localization. Fucosylated glycans, including both outer-arm and core-fucosylated species, were notably more abundant in tumor compared to normal tissue. These glycans are believed to play roles in immune modulation, cell adhesion, and tumor–stromal communication. Their spatial enrichment in prostate cancer regions suggests a shift in fucosylation dynamics, possibly due to upregulation of fucosyltransferases such as FUT8. This pattern has been interpreted as possibly reflecting tumor-driven remodeling of glycosylation to facilitate immune evasion, altered signaling, or extracellular matrix interactions.

Taken together, these heatmaps underscore that glycan alterations in cancer are spatially highly differentiated, with normal tissues displaying structured and region-specific glycan distributions — especially in the stroma — that are lost or diminished in tumors. This highlights the potential of spatial glycoproteomics not only to identify tumor-specific glycan signatures but also to provide insight into the underlying cellular and microenvironmental reprogramming during malignancy.

To explore the cognate carrier protein underlying the glycan distributions observed by MALDI-MSI, we performed intact glycopeptide analysis on adjacent tissue sections using HILIC enrichment and glyco-PASEF. This approach enabled site-specific identification of glycopeptides with confident glycan composition and protein assignment.

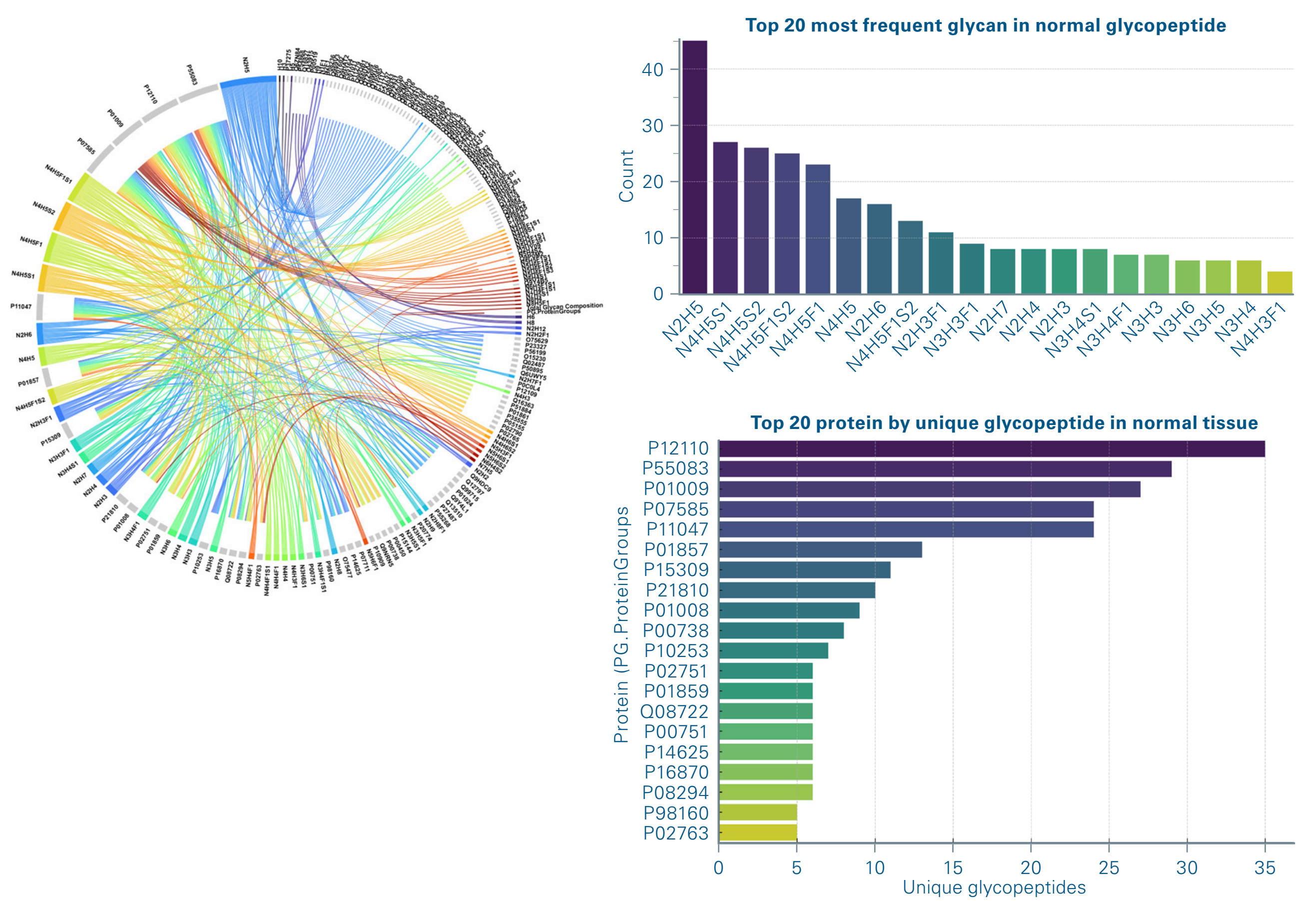

Figure 3.
Chord diagram and bar plots summarizing glycopeptide diversity and distribution in normal tissue.

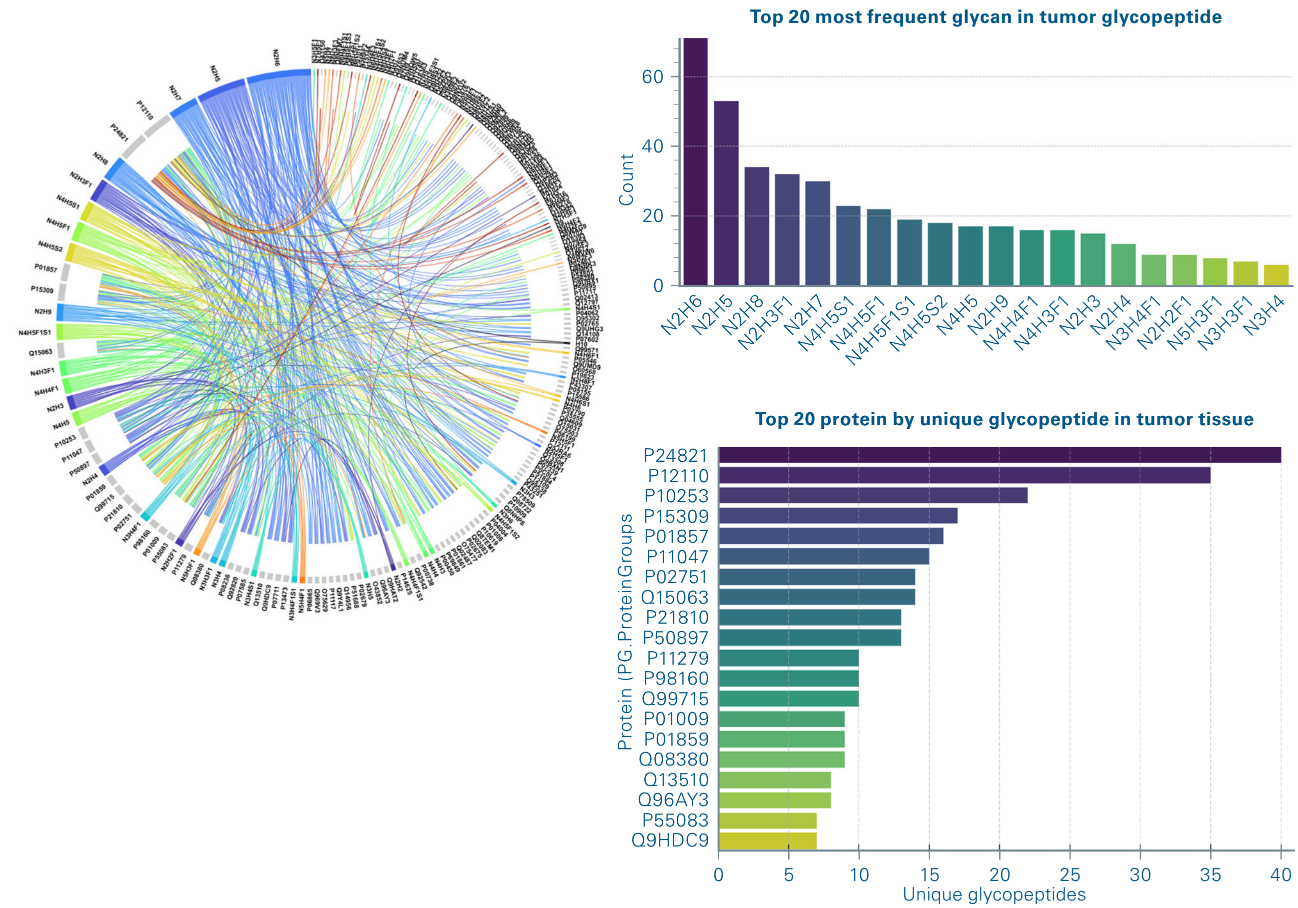

Figure 4.
Chord diagram and bar plots summarizing glycopeptide diversity and distribution in tumor tissue.

Across the dataset, a total of 59 distinct glycan compositions were detected, spanning complex, hybrid, and high-mannose types. Notably, the tumor tissue yielded a higher number of unique glycopeptides than the normal region, indicating either higher glycoprotein expression or greater glycan heterogeneity in the tumor microenvironment as compared to normal tissue. Chord diagram visualization (Figure 3 and 4) highlighted that certain glycans—such as N2H6, N2H8, N2H3F1, N2H7, were broadly distributed across more carrier-proteins in the tumor compared to the normal tissue. This suggests a possible expansion in glycan–protein connectivity in tumors, reflective of glycosylation remodeling.

Among the top glycoproteins identified were serine protease inhibitors, complement factors, and structural proteins, many of which are known to be involved in cancer-related pathways. Importantly, the ability to assign glycan types to individual glycoproteins as well as glycosylation sites revealed patterns consistent with spatial glycomic trends observed earlier. For example, hybrid-type glycans, which were enriched in the stroma of normal tissues, were predominantly carried by extracellular matrix and plasma proteins.

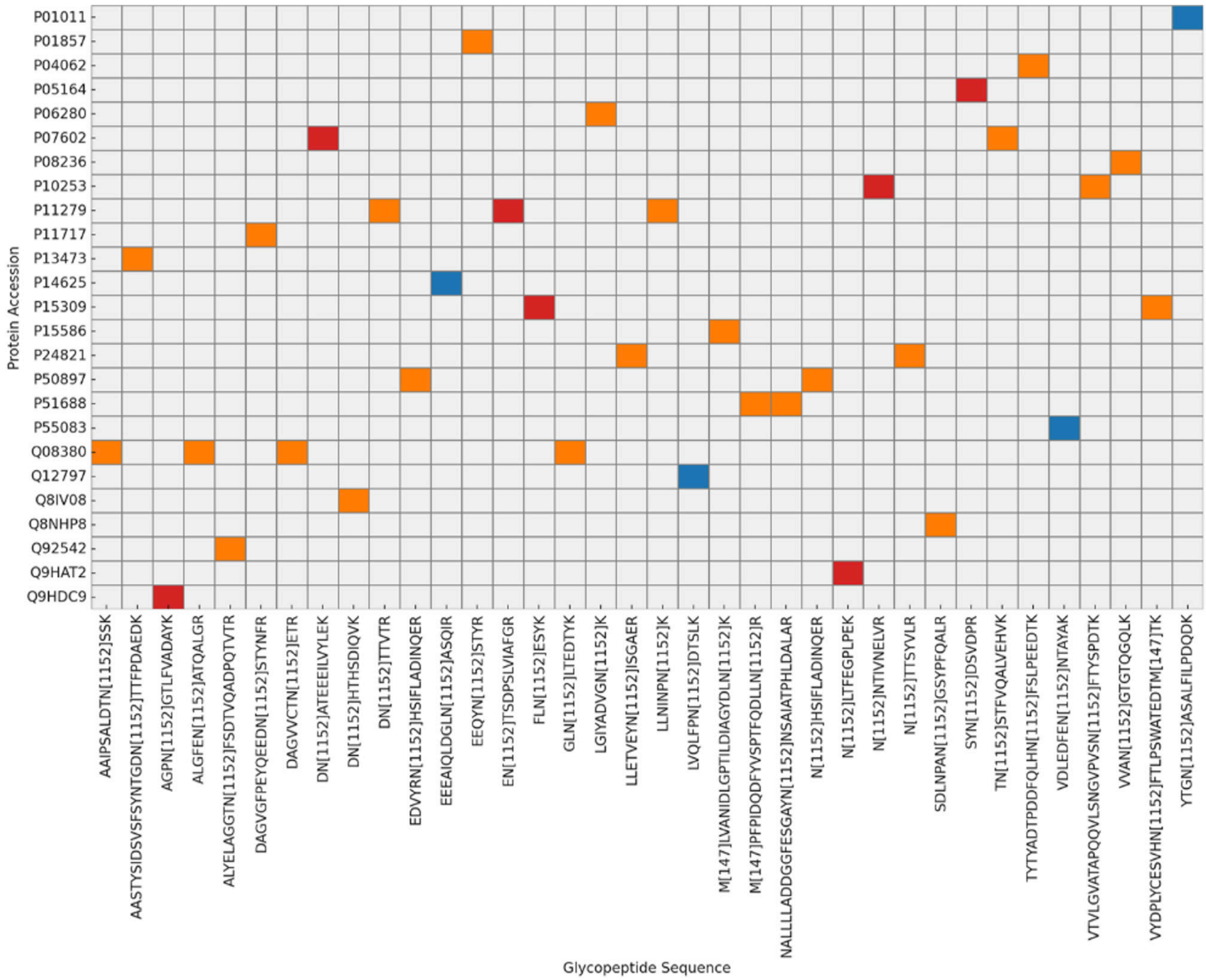

Figure 5.

Site- and protein-specific mapping of the glycoform N2H3F1 (HexNAc(2)Hex(3)Fuc(1)) across tumor (orange) and normal (blue) tissue.

To further examine site-specific glycosylation in tumor tissue, we focused on the glycoform N2H3F1 (HexNAc(2)Hex(3)Fuc(1)), which exhibited both distinguishable spatial distribution in MALDI-MSI and extensive heterogeneity at the peptide and protein levels in glycopeptide LC-MS/MS data. A total of 36 distinct protein–glycopeptide pairings were observed, including 25 tumor-specific, 4 normal-specific, and 7 shared between conditions. This diversity was visualized in a condition-colored heatmap, revealing that several prostate cancer-relevant proteins — such as CD59 glycoprotein (Q08380), Fibronectin (P24821), CEACAM5 (P11279), and the Androgen receptor (P10253) — carried multiple N2H3F1-modified peptides exclusively or predominantly in tumor tissue.

These findings underscore the value and remarkable additional insights that analyzing glycopeptides rather than just released glycans in isolation can afford. While imaging-based glycan detection can reveal broad spatial trends, it does not identify the underlying protein carriers or specific glycosylation sites, which are essential to understanding biological function, disease relevance, and therapeutic accessibility. By resolving which peptides and which proteins carry a given glycoform, glycopeptide LC-MS/MS adds critical molecular context to spatial glycomics and enables precise linkage between glycosylation changes and specific tumor-associated pathways.

Conclusions

By integrating MALDI-MSI with glycopeptide LC-MS/MS, we achieved spatial and molecular characterization of glycosylation in prostate cancer. MALDI-MSI revealed tumor-associated shifts in glycan distribution, while LC-MS/MS identified site-specific glycopeptide heterogeneity. The glycoform N2H3F1 (HexNAc(2)Hex(3)Fuc(1)) exemplified this, showing tumor-enriched spatial patterns and diverse protein–peptide mappings, including on cancer-relevant proteins such as CD59, Fibronectin, CEACAM5, and the Androgen receptor. These results underscore the value of combining imaging and glycoproteomics to un-cover biologically meaningful glycosylation changes in cancer.

References

[1] Mukherjee S, Jankevics A, Busch F, et al. (2023). *Oxonium Ion–Guided Optimization of Ion Mobility–Assisted Glycoproteomics on the timsTOF Pro*. Mol Cell Proteomics. **22**(2):100486.

[2] Baerenfaenger M, Post MA, Zijlstra F, et al. (2024). *Maximizing Glycoproteomics Results through an Integrated Parallel Accumulation Serial Fragmentation Workflow*. Anal Chem. **96**(22):8956–8964.

[3] Zhu J, Lin YH, Dingess KA, Mank M, Stahl B, Heck AJR. (2020). *Quantitative Longitudinal Inventory of the N-Glycoproteome of Human Milk from a Single Donor Reveals the Highly Variable Repertoire and Dynamic Site-Specific Changes*. J Proteome Res. **19**(5):1941–1952.

[4] Drake RR, Powers TW, Jones EE, Bruner E, Mehta AS, Angel PM. (2017). *MALDI Mass Spectrometry Imaging of N-Linked Glycans in Cancer Tissues*. Adv Cancer Res. **134**:85–116.

[5] Wallace EN, West CA, McDowell CT, et al. (2024). *An N-glycome tissue atlas of 15 human normal and cancer tissue types determined by MALDI-imaging mass spectrometry*. Sci Rep. **14**:489.

[6] Conroy LR, Stanback AE, Young LEA, et al. (2021). *In Situ Analysis of N-Linked Glycans as Potential Biomarkers of Clinical Course in Human Prostate Cancer*. Mol Cancer Res. **19**(10):1727–1738.

Bruker Switzerland AG

Fällanden · Switzerland
Phone +41 44 825 91 11

Bruker Scientific LLC

Billerica, MA · USA
Phone +1 (978) 663-3660

ms.sales.bdal@bruker.com – www.bruker.com